Electronic structure of $CaMnO_x$ with $2.66 \leqslant x \leqslant 3.00$ studied with photoemission and x-ray-absorption spectroscopy

G. Zampieri, F. Prado, A. Caneiro, J. Briático, M. T. Causa, M. Tovar, and B. Alascio
Centro Atómico Bariloche and Instituto Balseiro, Comisión Nacional de Energía Atómica and Universidad Nacional de Cuyo, 8400-San Carlos de Bariloche, Argentina

M. Abbate
Laboratorio Nacional de Luz Sincrotron, Conselho Nacional de Desenvolvimento Cientifico e Tecnologico, Caixa Postal 6192, 13083-970 Campinas SP, Brazil

E. Morikawa
Center for Advanced Microstructures and Devices, Louisiana State University, 3990 West Lakeshore Drive, Baton Rouge, Louisiana 70803
(Received 7 January 1998)

We studied the electronic structure of $CaMnO_x$ ($2.66 \leqslant x \leqslant 3.00$) using x-ray photoemission and O $1s$ x-ray-absorption spectroscopy. Analyzing the spectra of the two end members with the configuration-interaction cluster model, we have determined all the main parameters of the electronic structure. We have found that the ground states of $CaMnO_{2.5}$ and $CaMnO_3$ are highly covalent, with approximately the same number of ligand holes per oxygen atom: 0.22–0.23. The main separations between the Mn $3d$ bands closest to the Fermi level are of the order of 3 eV and the band gaps are of the charge-transfer type ($U > \Delta$). The main effects of the oxygenation are the disappearance of the occupied $e_{g\uparrow}$ band and an approximately rigid shift of about 1 eV to lower energies of all the other Mn $3d$ bands. Finally, we discuss the most probable causes for the absence of a metallic phase in $CaMnO_x$. [S0163-1829(98)01427-1]

I. INTRODUCTION

The great variety of physical properties of ABO_3 oxides with perovskite structures has made them a lively area of research in the last decade. Among these compounds, the series $La_{1-x}Ca_xMnO_3$ has attracted much attention recently due to the discovery of colossal magnetoresistance effects.[1–4] Both end members of this series are insulators and antiferromagnetic at low temperatures, but when trivalent La is replaced by divalent Ca (or Sr or Ba) in the range $0.2 \leqslant x \leqslant 0.4$, the material becomes a metallic ferromagnet.[5] From the electronic point of view the doped compounds are mixed-valent systems with a disordered distribution of Mn^{3+} and Mn^{4+} ions. The strong coupling between the magnetic ordering and the electrical conductivity is explained by the double-exchange model,[6,7] in which the electrons in e_g orbitals are the electrical carriers that move on a background of $Mn^{4+}(t_{2g}^3)$ ions. The alignment of the Mn^{4+} localized spins favors the delocalization of the e_g electrons and reduces the total energy of the system. Mixtures of Mn^{3+} and Mn^{4+} ions can also be produced increasing the oxygen content in $LaMnO_3$ or reducing it in $CaMnO_3$, although in this last case the Mn^{3+} ions are no longer in the regular octahedral coordination but in square pyramidal coordination. However, these two approaches lead to different results: $LaMnO_{3+\delta}$ becomes a metallic ferromagnet for $\delta = 0.12 - 0.17$ (Ref. 8) whereas $CaMnO_{3-\delta}$ remains an insulator over the range $0 \leqslant \delta \leqslant 0.33$.[9]

The electronic structure of $La_{1-x}Ca_xMnO_3$ has been investigated both theoretically and experimentally.[10–18] Most of the experimental studies have been performed using x-ray photoemission spectroscopy (XPS) to probe the occupied electronic states[10,11,13,14,17] and X-ray absorption[12,14] (XAS) or bremsstrahlung isochromat spectroscopies[13] to probe the empty electronic states. The analysis of these spectra with a configuration-interaction (CI) model[19] allows a determination of important parameters such as U (the on-site d-d Coulomb energy), Δ (the p-d charge-transfer energy), and T (the p-d hybridization energy), and a classification of the compound as Mott-Hubbard ($U < \Delta$) or a charge-transfer ($U > \Delta$) insulator. At present there is some controversy on whether $LaMnO_3$ and $CaMnO_3$ are in the Mott-Hubbard[13] or charge-transfer regime.[14] In this paper we report a study of the electronic structure of $CaMnO_x$ with x in the range $2.66 \leqslant x \leqslant 3.00$. Despite the compounds in this series also being a mixture of Mn^{3+} and Mn^{4+} ions, as mentioned above, they become neither metallic nor ferromagnetic for any composition.[9] Measuring the XPS valence-band and O $1s$ XAS spectra we determine the changes in the occupied and empty bands induced by the oxygenation, and analyzing these spectra and the Mn $2p$ spectra of the end members ($CaMnO_{2.5}$ and $CaMnO_3$) using the CI cluster model we determine all the main parameters of the electronic structure: U, Δ, T, J (the on-site d-d exchange energy), and $10Dq$ and Ds (the crystal-field parameters of a d level in octahedral and pyramidal symmetry, respectively).

II. EXPERIMENTAL DETAILS

The samples studied in this work were $CaMnO_x$ with $x = 2.66$, 2.75, 2.84, and 3.00. The $CaMnO_3$ sample was pre-

pared by the standard nitrate method. The resulting powder was pressed into pellets and sintered in air at 1400 °C. The other samples were obtained by reducing the $CaMnO_3$ sample in a thermogravimetric balance at 1000 °C. The metastable $CaMnO_{2.84}$ and $CaMnO_{2.66}$ samples were obtained for O_2 partial pressures of 10^{-2} and 10^{-4} atm, respectively. The $CaMnO_{2.75}$ sample was prepared at 10^{-3} atm and quenched at the desired composition. The $CaMnO_{2.5}$ sample could not be produced using our experimental setup.

The crystalline structure of $CaMnO_x$ with $2.50 \leqslant x \leqslant 3.00$ is related to a distorted variation of the cubic perovskite.[20] The oxygen deficiency in the compound is accommodated by the presence of vacancies at the oxygen sites. $CaMnO_x$ is an insulator for any oxygen concentration in the range $2.66 \leqslant x \leqslant 3.00$; the electrical conductivity first increases with x and then decreases, reaching at $x=3.00$ a value close to that of the sample with $x=2.66$.[9]

The XPS spectra were taken with an Al $K\alpha_{1,2}$ source ($h\nu=1486.6$ eV) and a hemispherical energy analyzer ($r=10$ cm). All the spectra have been corrected for the Al $K\alpha_{3,4}$ ghost lines. The core levels and Fermi edges of clean Ni and Cu samples were used in the experiments to calibrate the energy scale. The total energy resolution was estimated to be 1.0 eV. All the samples were scraped with a diamond file prior to their insertion into the spectrometer chamber. Survey XPS spectra showed only a small residual contamination with C, whereas the O 1*s* peaks were similar to those reported in previous works.[14]

The XAS spectra were taken using the plane grating monochromator at CAMD. The spectra were taken in the total electron yield mode measuring the current emitted by the sample. The throughput of the monochromator was determined with a calibrated photodiode and used to normalize the intensity. The energy scale was calibrated using the known peak positions in NiO and in CuO. The energy resolution at the O 1*s* edge (around 530 eV) was approximately 0.6 eV. To obtain fresh, clean surfaces, all the samples were scraped inside the vacuum chamber prior to the measurements using a diamond file.

III. RESULTS

A. XPS and XAS spectra

Figure 1 shows the XPS spectra in the region of the Mn $2p$ level. All the spectra exhibit the usual $2p_{1/2}$ and $2p_{3/2}$ spin-orbit doublet. It is seen in the figure that the $2p_{3/2}$ peak appears at the same energy (-641.9 eV) in all the compounds, and so no chemical shift is apparent in agreement with previous studies.[13,14] However, when the energy is referred to the position of the Ca $3p$ level, assumed to be a constant reference level (see below), the peak in $CaMnO_3$ does show a chemical shift of 0.4 eV to higher binding energies. The $2p_{1/2}$ peak is at 11.5 eV from the main peak and a weak structure is observed at about 23.7 eV in $CaMnO_3$ and at about 23.2 eV in $CaMnO_{2.66}$. As in previous works, we ascribe this structure to a satellite of the $2p_{1/2}$ peak. This means that the satellite of the $2p_{3/2}$ peak must be overlapping with the $2p_{1/2}$ peak. This, in turn, explains why the intensity ratios $I(2p_{1/2}):I(2p_{3/2})$ exceed the expected 1:2 ratio.

The XPS spectra in the region of the valence levels are shown in Fig. 2. The intense peak and the shoulder in the region between -25 and -20 eV correspond to photoelectrons from the Ca $3p$ and O $2s$ levels, respectively. It is seen that in $CaMnO_3$ both structures are shifted 0.4 eV towards the Fermi level. As this same shift is also observed in the

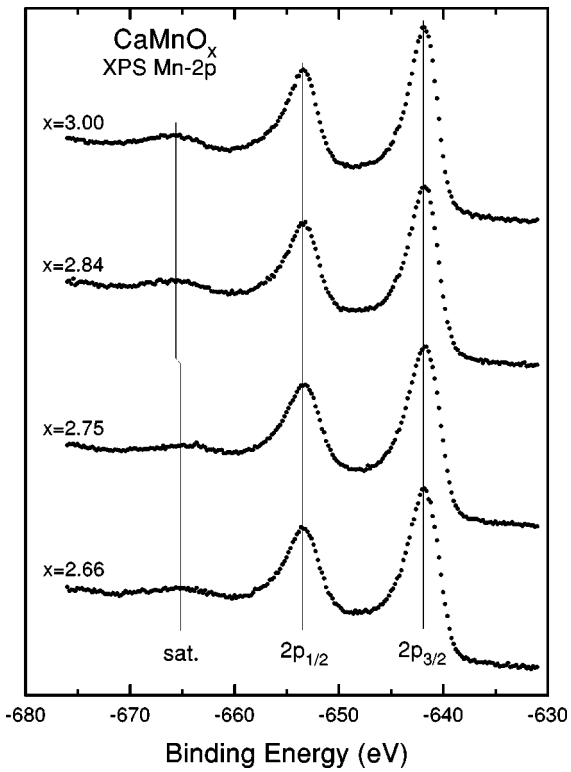

FIG. 1. XPS Mn $2p$ spectra of $CaMnO_x$.

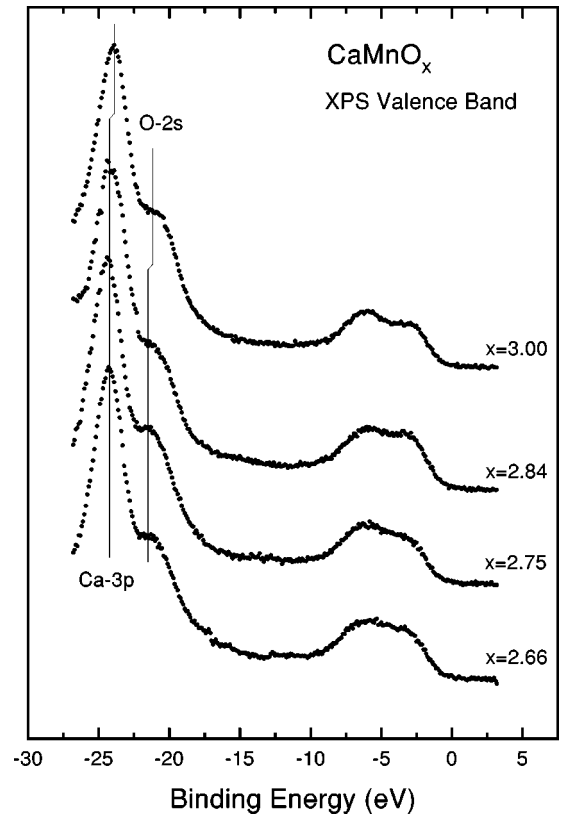

FIG. 2. XPS valence-band spectra of $CaMnO_x$.

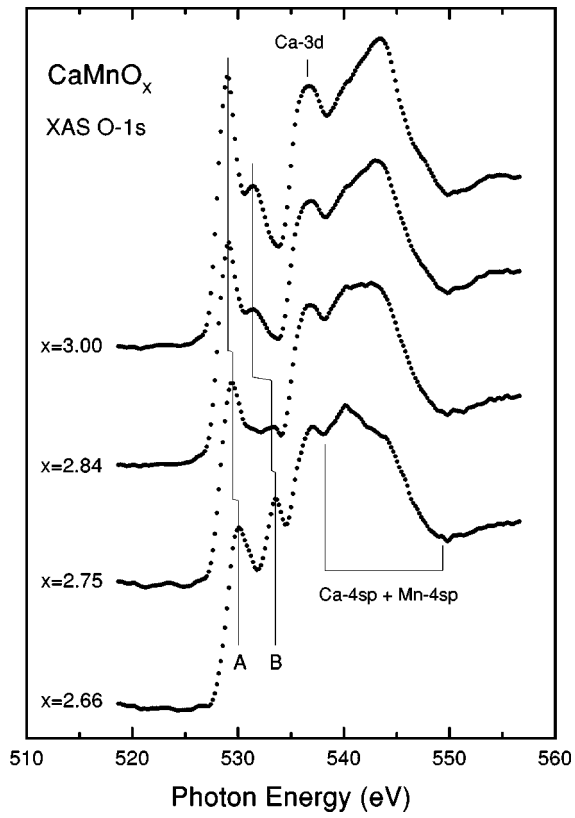

FIG. 3. XAS O 1s spectra of $CaMnO_x$.

case of the O 1s level, and considering that these levels are not expected to be chemically shifted, we ascribe this shift in $CaMnO_3$ to a shift of the Fermi level in the band gap. The broad structure between -10 eV and 0 comprises the contributions from the O 2p and Mn 3d levels, which at $h\nu=1486.6$ eV have similar weights.[21] No structure is observed in the region between -17 and -9 eV. This means that the satellites that are expected to accompany the Mn 3d photoemission must be separated from the main contribution at least 10–12 eV, which is consistent with the satellite energies determined in the case of the Mn 2p photoemission.

The XAS spectra in the region of the O 1s edge, presented in Fig. 3, are the ones that exhibit the largest changes with x. These spectra correspond to electronic transitions from the O 1s level into unoccupied levels in the conduction band with some O 2p character. The two peaks close to threshold (labeled A and B) are attributed to transitions into empty bands with majority Mn 3d character. The peak at around 537 eV is assigned to states with majority Ca 3d character, and the broad structure between 538 and 550 eV is attributed to a band with mixed Mn 4sp and Ca 4sp character. It is observed in Fig. 3 that the two peaks close to threshold shift to lower energies when x increases. This shift is accompanied by a loss of intensity of the peak labeled B, which is due simply to the increasing separation of this peak from the steep edge of the Ca 3d peak, and by an intensity gain of the peak labeled A, which is attributed to an increase of the density of states at the bottom of the conduction band when x increases.

B. Configuration-interaction cluster model

In this section we will compare spectra calculated within the CI cluster model for the end members $CaMnO_3$ and $CaMnO_{2.5}$ with the experimental spectra corresponding to the samples $CaMnO_3$ and $CaMnO_{2.66}$, respectively.

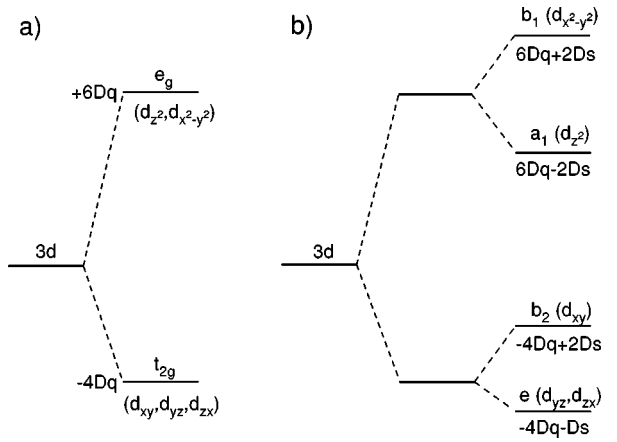

FIG. 4. Energy level diagrams showing the crystal-field splitting of a d level in (a) octahedral symmetry and (b) pyramidal symmetry (Ref. 22).

The CI cluster model has been found to provide a good first-order description of the electronic structure of most TM compounds. In this model one neglects the translational symmetry of the crystal and solves the problem of a cluster made of the central cation plus its nearest-neighbor anions. The ground state (GS) of the cluster is described as a mixture of the ionic d^n state and the charge-transfer $d^{n+1}\underline{L}$ and $d^{n+2}\underline{L}^2$ states, where n is the nominal d-electron number of the TM (3 in $CaMnO_3$ and 4 in $CaMnO_{2.5}$) and $\underline{L}$ denotes a ligand hole.

The energies of the centers of gravity of the d^n, $d^{n+1}\underline{L}$, and $d^{n+2}\underline{L}^2$ multiplets are set equal to 0, Δ, and $2\Delta+U$, respectively, with Δ the charge-transfer energy and U the average Coulomb repulsion energy (including exchange). Following Bocquet *et al.*[11] we have written the energies of the d^n, d^{n+1}, and d^{n+2} configurations of the TM ion (with respect to the centers of gravity of the multiplets) in terms of three parameters. These are $u=\langle\phi_{3d\uparrow}\phi_{3d\downarrow}|H|\phi_{3d\uparrow}\phi_{3d\downarrow}\rangle$, the Coulomb repulsion between two d electrons in the same orbital, $u'=\langle\phi_{3d}\psi_{3d}|H|\phi_{3d}\psi_{3d}\rangle$, the Coulomb repulsion between two d electrons in different orbitals, and $J=\langle\phi_{3d}\psi_{3d}|H|\psi_{3d}\phi_{3d}\rangle$, the exchange interaction. Further, since the TM ion is surrounded by negative ions, we have also considered the electrostatic crystal-field splitting of the d levels. The splittings appropriate for a TM ion in octahedral ($CaMnO_3$) and pyramidal ($CaMnO_{2.5}$) symmetries are illustrated in Figs. 4(a) and 4(b). This completes the list of parameters used to define the energies of the different configurations. Note, however, that the parameters U, u, u', and J are not independent, as they are related by $u-u'=2J$ and $u-U=\frac{2}{9}J$.

The ligand-p–TM-d interactions are taken into account through the one-electron transfer integrals $T_\alpha=\langle d_\alpha|H|L_\alpha\rangle$, where d_α and L_α are a TM-d orbital and a combination of ligand-p orbitals with the same symmetry. In $CaMnO_{3.0}$, where the Mn^{4+} ions are in sites of octahedral symmetry, one has two parameters: $T_\pi=2(pd\pi)$ and $T_\sigma=\sqrt{3}(pd\sigma)$. In $CaMnO_{2.5}$, where the Mn^{3+} ions occupy sites with square pyramidal oxygen coordination, there are four different hy-

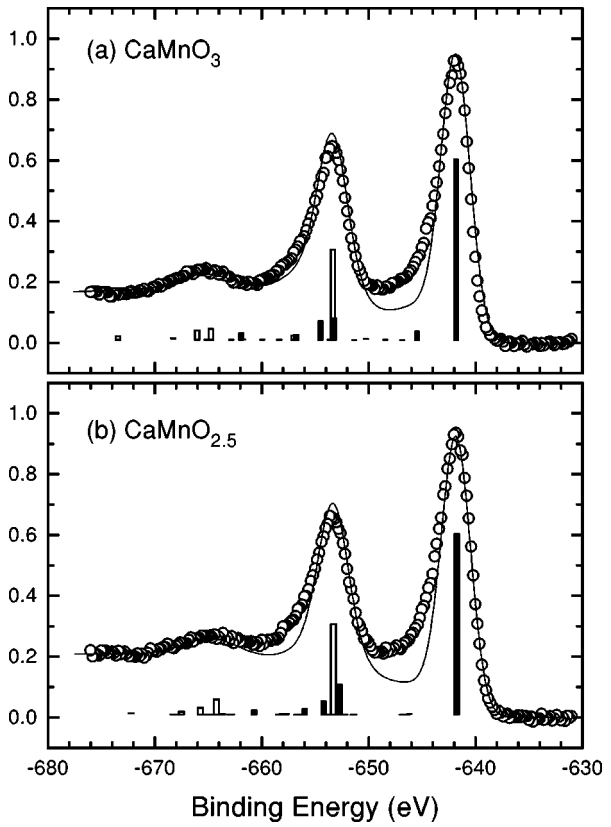

FIG. 5. Comparison of the experimental and calculated XPS Mn $2p$ spectra of (a) $CaMnO_3$ and (b) $CaMnO_{2.5}$. The solid and hollow bars represent the $2p_{3/2}$ and $2p_{1/2}$ final states, respectively.

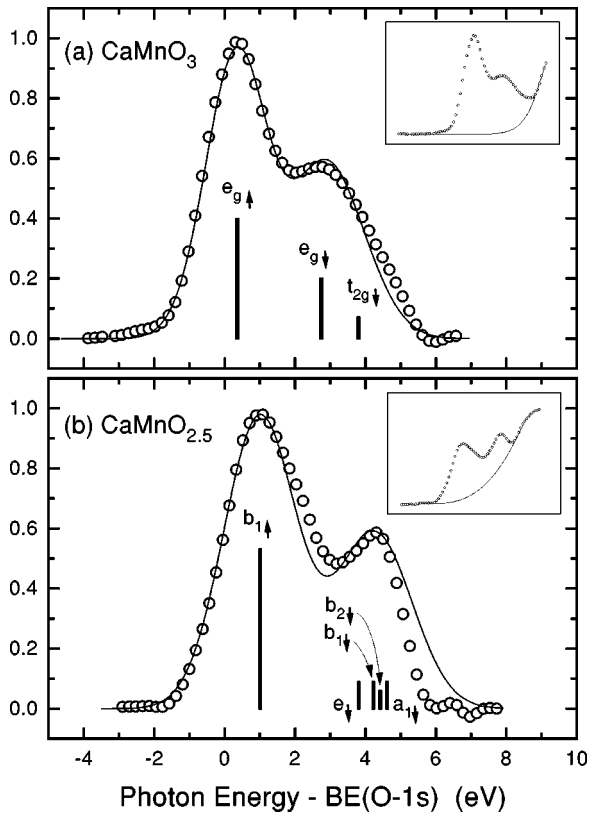

FIG. 6. Comparison of the experimental and calculated XAS O $1s$ spectra of (a) $CaMnO_3$ and (b) $CaMnO_{2.5}$. The insets show the background curves that have been subtracted from the measured spectra.

bridization integrals: $T_{\pi 1}=\sqrt{3}(pd\pi)$, $T_{\pi 2}=2(pd\pi)$, $T_{\sigma 1}=\frac{2}{3}\sqrt{3}(pd\sigma)$, and $T_{\sigma 2}=\sqrt{3}(pd\sigma)$.

The XPS Mn $2p$ spectra require an additional parameter: $Q=\langle\phi_{2p}\psi_{3d}|H|\phi_{2p}\psi_{3d}\rangle$, the interaction of a d electron with the $2p$ core hole, which has been set equal to $U/0.83$. We have also set $(pd\sigma)/(pd\pi)\approx -2.2$, as in previous studies.[11,14] Therefore, the total number of adjustable parameters has been 5 in $CaMnO_3$: Δ, U, J, $(pd\sigma)$, and $10Dq$, and 6 in $CaMnO_{2.5}$ (the same parameters plus Ds).

In Figs. 5–7 we compare the experimental spectra with the spectra calculated with the CI cluster model, and in Table I we list the parameters that yield the best fittings. $\Delta_{\rm eff}$ and $U_{\rm eff}$ are the charge-transfer and average Coulomb energies defined with respect to the lowest-energy states of the multiplets.

The fitting procedure has been as follows. We have found that the position of the satellite in the Mn $2p$ spectra is a strong function of $(pd\sigma)$, whereas its intensity is determined mainly by U. Therefore, we have first set $(pd\sigma)$ and U to reproduce the position and intensity of the Mn $2p$ satellite. Then, using these values we varied J and $10Dq$ (and Ds in $CaMnO_{2.5}$) until a good fit to the XAS spectrum was obtained. Finally, Δ was used to control the gap energy and through it the position of the Mn $3d$ contribution in the XPS valence-band spectra.

Figures 5(a) and 5(b) show the best fits to the experimental Mn $2p$ spectra. The calculated spectra have been broadened with a Lorentzian function whose width increases with the energy and convoluted with a Gaussian function to simulate the experimental broadening. To ease the comparison we have subtracted a linear background to the experimental spectra and we have added a steplike loss function to the calculated spectra. The position and relative intensity of the satellite (at about 12 eV from the $2p_{1/2}$ peak) are very well reproduced in both calculations. As mentioned above, the position of the satellite depends sensitively on $(pd\sigma)$; this allows a determination of this parameter with an accuracy of about ± 0.1 eV. In both compounds, the most important contributions to the main (*well-screened*) peak come from $\underline{c}d^{n+1}\underline{L}$ final states, whereas in the case of the satellite (*poorly screened)* peak the main contributions come from $\underline{c}d^{n}$ and $\underline{c}d^{n+1}\underline{L}$ final states.

The region of the XAS O $1s$ spectra corresponding to the empty bands with majority Mn $3d$ character are shown in Figs. 6(a) and 6(b). In the experimental spectra we have subtracted the background curves that are shown in the insets of the figures and have referenced the energies to the O $1s$ XPS binding energies. The calculated spectra were shifted by hand until a good agreement with the experimental spectra was obtained. In the calculations we have neglected the interaction of the core hole with the valence electrons; therefore, the final states are directly the addition states (AS) of the system. In $CaMnO_3$ there are three AS's; they have been labeled in Fig. 6(a) after the orbitals occupied by the electron added to the system. The energy differences between these AS's are very close to $3J$ and $2J-10Dq$, and their intensities are given essentially by the occupancies of the configurations $|t_{2g\uparrow}^3 e_{g\uparrow}\underline{L}_{\sigma\downarrow}\rangle$, $|t_{2g\uparrow}^3 e_{g\downarrow}\underline{L}_{\sigma\uparrow}\rangle$, and $|t_{2g\uparrow}^3 t_{2g\downarrow}\underline{L}_{\pi\uparrow}\rangle$ in the GS. In $CaMnO_{2.5}$, due to the lower symmetry, there are five

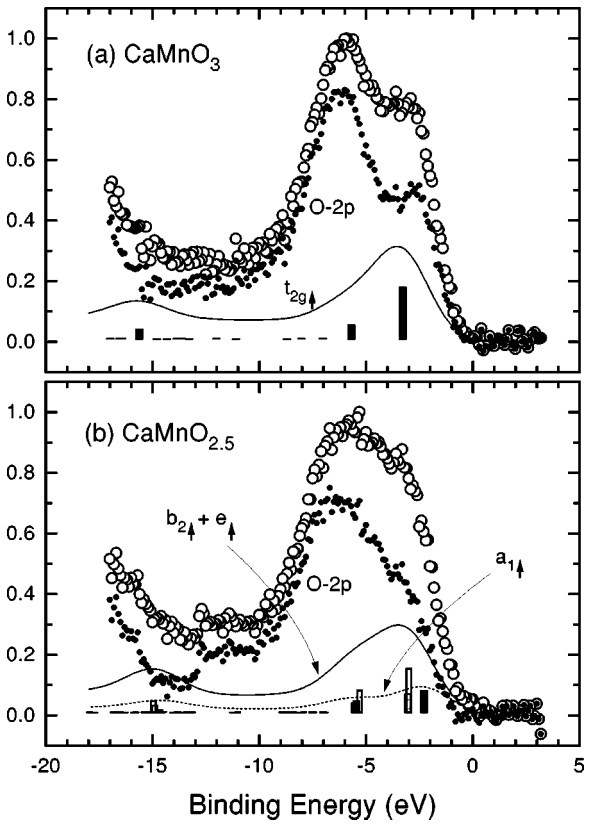

FIG. 7. Decomposition of the XPS valence-band spectra of (a) $CaMnO_3$ and (b) $CaMnO_{2.5}$ into Mn $3d$ and O $2p$ contributions. In $CaMnO_{2.5}$ the solid, striped, and hollow bars are the final states corresponding to the photoemission of an electron from the $a_{1\uparrow}$, $b_{2\uparrow}$, and $e_{\uparrow}$ orbitals, respectively.

AS's; they correspond to adding an electron in the $b_{1\uparrow}$, $e_{\downarrow}$, $b_{1\downarrow}$, $b_{2\downarrow}$, and $a_{1\downarrow}$ orbitals. The energy differences between these states are close to $6J-10Dq-3Ds$, $10Dq+3Ds-2J$, $2J-10Dq$, and $10Dq-4Ds$. As in $CaMnO_3$, the intensities are dictated mainly by the occupancies of the corresponding $d^5\underline{L}$ configurations in the GS. According to Figs. 6(a) and 6(b), the energies of the first AS's in $CaMnO_3$ and $CaMnO_{2.5}$ are 0.3 and 1.0 eV above the Fermi level, respectively.

Finally, Figs. 7(a) and 7(b) present the decomposition of the experimental XPS valence-band spectra into the Mn $3d$ and O $2p$ contributions. The Mn $3d$ contributions have been calculated using the parameters obtained in the fittings described above, and the O $2p$ contributions have been obtained subtracting the Mn $3d$ contributions from the measured spectra.[23] As in the case of the Mn $2p$ spectra, we have subtracted a linear background to the experimental spectra and added a steplike loss function to the broadened calculated spectra. The final states in the calculation of the Mn $3d$

TABLE I. Parameters obtained with the CI cluster model analysis of the spectra. All the quantities are in eV.

	Δ	U	$(pd\sigma)$	J	$10Dq$	Ds	Δ_{eff}	U_{eff}
$CaMnO_3$	2.0	7.8	-1.5	0.82	0.2		0.21	7.16
$CaMnO_{2.5}$	2.8	7.5	-1.8	0.75	0.3	0.05	0.75	11.7

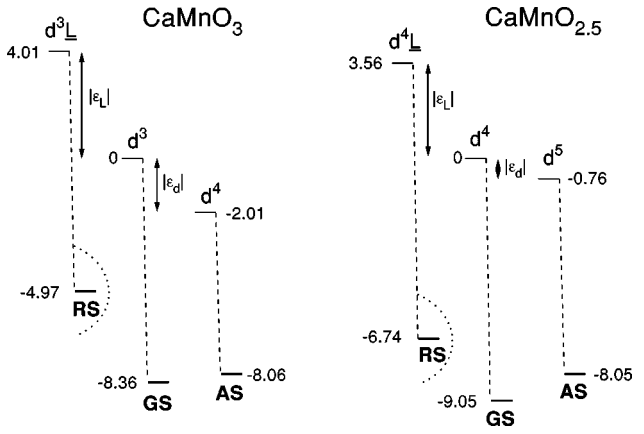

FIG. 8. Total-energy diagrams showing the first removal state (RS), ground state (GS), and first addition state (AS) of $CaMnO_3$ and $CaMnO_{2.5}$ prior to and after the hybridization.

contributions are the removal states (RS) of the system. The energy zeros in the calculated spectra have been defined so that the first RS appears at the energy of the first AS [taken from Figs. 6(a) and 6(b)] minus the gap energy. In $CaMnO_3$ all the final states correspond to the photoemission of an electron from a $t_{2g\uparrow}$ orbital. The most important contribution to the two intense final states in the region between -10 eV and 0 comes from configurations with $d^3\underline{L}$ character, whereas the most important contribution to the satellite comes from the configuration with d^2 character. In $CaMnO_{2.5}$ there are three types of final states. These correspond to the photoemission of an electron from the $a_{1\uparrow}$, $b_{2\uparrow}$, and $e_{\uparrow}$ orbitals. The first RS ($a_{1\uparrow}$) appears at -2.3 eV and, as in $CaMnO_3$, the main contribution to the final states in the energy region between -10 eV and 0 comes from $d^4\underline{L}$ configurations, while the main contribution to the satellite comes from the d^3 configurations.

IV. DISCUSSION

Having determined the parameters that yield the best fittings to the XPS and XAS spectra, we can use the CI cluster model to get a deeper insight into the electronic properties. Figure 8 presents the energy level diagrams corresponding to $CaMnO_3$ and $CaMnO_{2.5}$. The energies are referenced to the energies of the ionic configurations d^3 and d^4, which are the starting points in each calculation. We have set the energy differences between the first AS and the GS equal to the energies determined in Figs. 6(a) and 6(b). This determines the values of ε_d in each case and of $\varepsilon_L=\varepsilon_d-\Delta$.[19] Note that the hybridization energies in $CaMnO_{2.5}$ are about 2 eV larger than in $CaMnO_3$, in correspondence with the larger value of $(pd\sigma)$ in this compound.

From Fig. 8 it is immediately evident that the main effect of the oxygenation (of $CaMnO_{2.5}$) is to pull down the energy of the first AS and to lift up the energy of the first RS.

This is confirmed by the plots in Fig. 9 of the occupied and empty bands. The O $2p$ and Mn $3d$ occupied bands (below ε_F) are those of Figs. 7(a) and 7(b), while the empty bands (above ε_F) are those of Figs. 6(a) and 6(b). In the occupied Mn $3d$ bands we have omitted the steplike loss functions and we have corrected the O $2p$ bands for the

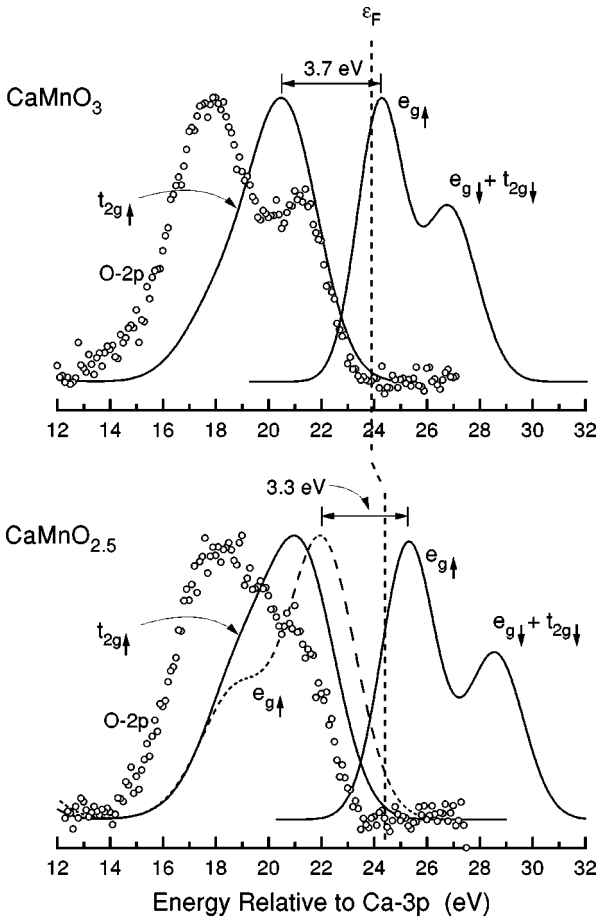

FIG. 9. Occupied and empty bands (not in scale) of $CaMnO_3$ and $CaMnO_{2.5}$ plotted as a function of the energy relative to the Ca $3p$ level. In $CaMnO_{2.5}$ the Mn $3d$ bands have been labeled neglecting the crystal-field splitting due to the pyramidal symmetry ($Ds=0$).

inelastic tails. Note also that, to ease the comparison, the Mn $3d$ bands in $CaMnO_{2.5}$ have been labeled neglecting the crystal-field splitting introduced by the pyramidal symmetry. All the bands have been plotted as a function of the energy relative to the Ca $3p$ level, which has been taken as a constant reference level. It is seen in this figure that the oxygenation of $CaMnO_{2.5}$ produces, apart from the disappearance of the occupied $e_{g\uparrow}$ band, a more or less rigid shift towards lower energies of all the Mn $3d$ bands. The empty $e_{g\uparrow}$ band shifts by 1.1 eV and the occupied $t_{2g\uparrow}$ band by 0.7 eV. It is seen that the shift of this latter causes its high-energy edge to nearly coincide with the high-energy edge of the O $2p$ band. It can be concluded from this figure that doping $CaMnO_3$ with electrons generates states of $e_{g\uparrow}$ symmetry at the top of the valence band and that, similarly, the doping of $CaMnO_{2.5}$ with holes induces unoccupied states of $e_{g\uparrow}$ symmetry at the bottom of the conduction band.

The gap energies, defined as $\varepsilon_{gap}=E_{RS}+E_{AS}-2E_{GS}$, are listed in Table II. They are similar in both compounds, in agreement with the resistivity vs T curves measured on these samples.[9] Note, however, that these gaps, which are 2–3 eV larger than those derived from the resistivity data, must be understood as the mean separation between the occupied and empty bands closest to the Fermi level. This is so because in our calculations we have neglected the dispersion of the O $2p$ states. Figure 8 shows that the inclusion of the O $2p$ bandwidth in the calculation of the RS should decrease the gap energy in approximately a half bandwidth, which is precisely of the order of 2–3 eV.

TABLE II. Gap energies (in eV), configuration occupancies, and numbers of d electrons and of ligand holes in the ground state.

	ε_{gap}	d^n	$d^{n+1}\underline{L}$	$d^{n+2}\underline{L}^2$	N_d^e	N_L^h
$CaMnO_3$	3.7	41.3	51.4	7.3	3.66	0.66
$CaMnO_{2.5}$	3.3	48.1	46.7	5.2	4.57	0.57

The reduced resistivity of the compounds with intermediate compositions[9] is assigned to the opening of the new charge-fluctuation channel: $d^4_{pyram}+d^3_{octah}\rightarrow d^3_{pyram}+d^4_{octah}$, which, according to Fig. 9, requires the order of 1.5 eV less energy.

In Table II we have also listed the occupancies of the different configurations in the GS and the numbers of d electrons N_d^e and ligand holes N_L^h. In both $CaMnO_3$ and $CaMnO_{2.5}$ the occupancies of the configurations d^n and $d^{n+1}\underline{L}$ are comparable, indicating a high degree of covalency. As expected, the occupancy of the $d^{n+1}\underline{L}$ configurations and the number of ligand holes increase upon oxygenation. Note, however, that the number of holes per oxygen atom is approximately the same in both compounds: 0.22–0.23.

An important issue concerning the carrier mobility in these compounds is the nature of the lowest-energy excitations. This can be examined with the help of the configuration occupancies in the first removal and addition states shown in Table III. As expected, the first AS's are dominated by the d^{n+1} configurations. This means that an electron added to the system will have a strong d character. On the contrary, in both compounds, the first RS's are dominated by the $d^n\underline{L}$ configurations, giving a majority ligand character to the holes added to the system. Moreover, it is seen from Table III that the ligand character of the holes increases with the oxygenation. Therefore, the lowest-energy excitations in $CaMnO_3$ and $CaMnO_{2.5}$ involve $d_i^n+d_j^n\rightarrow d_i^n\underline{L}+d_j^{n+1}$ transitions, and, consequently, the gaps are of the charge-transfer-type. This is in agreement with the Zaanen-Sawatzky-Allen classification scheme,[19] because in both compounds $U>\Delta$.

Therefore, the parameters and the main aspects of the electronic structure of $CaMnO_x$ are similar to those of $La_{1-x}Ca_xMnO_3$,[14] and so this opens the question of why $CaMnO_x$ does not have a metallic phase for intermediate x. The answer to this question is not clear yet, and more work is needed to clarify this point. We can conclude that it must not be related to the change of symmetry at the Mn site, as we have found that the crystal-field splitting plays only a minor

TABLE III. Configuration occupancies in the first removal (RS) and addition (AS) states.

	RS			AS	
	d^{n-1}	$d^n\underline{L}$	$d^{n+1}\underline{L}^2$	d^{n+1}	$d^{n+2}\underline{L}$
$CaMnO_3$	9.1	65.5	25.4	85.0	15.0
$CaMnO_{2.5}$	11.1	59.1	29.8	90.7	9.3

role. Two more likely explanations for the absence of a metallic phase are that the electrons added to the system remain localized by the potential of the oxygen vacancies, or that the small ionic radius of Ca induces a deviation of the Mn-O-Mn angle from 180° and a reduction of the transfer integral large enough to inhibit the delocalization of the electrons.

V. SUMMARY AND CONCLUSIONS

We have studied the electronic structure of $CaMnO_x$ with $2.66 \leqslant x \leqslant 3.00$ using x-ray photoemission and x-ray absorption spectroscopy. We have also analyzed the spectra of the two end members of the series with the configuration-interaction cluster model. The spectra of $CaMnO_{2.66}$ have been compared with those calculated for $CaMnO_{2.5}$ including the reduced symmetry at the Mn site.

We have obtained values for all the parameters that determine the electronic properties. We have found that in $CaMnO_3$ and $CaMnO_{2.5}$ the ground states are highly covalent, with approximately the same number of ligand holes per oxygen atom in both compounds: 0.22- 0.23. With regard to the occupied and empty electronic states, we have found that the main effect of the oxygenation is to shift all the Mn $3d$ bands (other than the occupied $e_{g\uparrow}$ band) by around 1 eV to lower energies. This determines that in $CaMnO_3$ the high-energy edge of the occupied $t_{2g\uparrow}$ band nearly coincides with the high-energy edge of the O $2p$ band. We have determined that the mean separation between the empty and occupied bands closest to the Fermi level is of the order of 3 eV, and that the gaps in $CaMnO_3$ and $CaMnO_{2.5}$ are of the charge-transfer type.

[1] R. Von Helmolt, J. Wecker, B. Holzapfel, L. Schultz, and K. Samwer, Phys. Rev. Lett. **71**, 2331 (1993).

[2] Y. Tokura, A. Urushivara, Y. Morimoto, T. Arima, A. Asamitsu, G. Kido, and N. Furukawa, J. Phys. Soc. Jpn. **63**, 3931 (1994).

[3] S. Jin, T. H. Tiefel, M. McCormack, R. A. Fastnacht, P. Ramesh, and L. H. Chen, Science **264**, 413 (1994).

[4] P. Schiffer, A. P. Ramirez, W. Bao, and S.-W. Cheong, Phys. Rev. Lett. **75**, 3336 (1995).

[5] G. H. Jonker and J. H. Van Santen, Physica (Amsterdam) **16**, 337 (1950); J. H. Van Santen and G. H. Jonker, *ibid.* **16**, 599 (1950).

[6] C. Zener, Phys. Rev. **82**, 403 (1951).

[7] P.G. De Gennes, Phys. Rev. **118**, 141 (1960).

[8] R. Mahendiran, S. K. Tiwary, A. K. Raychaduri, T. V. Ramakrisnan, R. Makesh, N. Raganvittal, and C. N. R. Rao, Phys. Rev. B **53**, 3348 (1996); C. N. R. Rao and A. K. Cheetham, Science **272**, 369 (1996).

[9] J. Briático, B. Alascio, R. Allub, A. Butera, A. Caneiro, M. T. Causa, and M. Tovar, Phys. Rev. B **53**, 1 (1996).

[10] D. J. Lam, B. W. Veal, and D. E. Ellis, Phys. Rev. B **22**, 5730 (1980).

[11] A. E. Bocquet, T. Mizokawa, T. Saitoh, H. Namatame, and A. Fujimori, Phys. Rev. B **46**, 3771 (1995).

[12] M. Abbate, F. M. F. de Groot, J. C. Fuggle, A. Fujimori, O. Strebel, F. Lopez, M. Domke, G. Kaindl, G. A. Sawatzky, M. Takano, Y. Takeda, H. Eisaki, and S. Uchida, Phys. Rev. B **46**, 4511 (1992).

[13] A. Chainani, M. Mathew, and D. D. Sarma, Phys. Rev. B **47**, 15 397 (1993).

[14] T. Saitoh, A. E. Bocquet, T. Mizokawa, H. Namatame, A. Fujimori, M. Abbate, Y. Takeda, and M. Takano, Phys. Rev. B **51**, 13 942 (1995).

[15] D. D. Sarma, N. Shanti, S. R. Barman, N. Hamada, H. Sawada, and K. Terakura, Phys. Rev. Lett. **75**, 1126 (1995).

[16] S. Satpathy, Z. S. Popović, and F. R. Vukajlović, Phys. Rev. Lett. **76**, 960 (1996).

[17] J.-H. Park, C. T. Chen, S.-W. Cheong, W. Bao, G. Meigs, V. Chakarian, and Y. U. Idzerda, Phys. Rev. Lett. **76**, 4215 (1996).

[18] J. H. Jung, K. H. Kim, D. J. Eom, T. W. Noh, E. J. Choi, J. Yu, Y. S. Kwon, and Y. Chung, Phys. Rev. B **55**, 15 489 (1997).

[19] J. Zaanen, G. Sawatzky, and J. Allen, Phys. Rev. Lett. **55**, 418 (1985).

[20] K. R. Poppelmeier, M. E. Leonowicz, and J. M. Longo, J. Solid State Chem. **44**, 89 (1982); A. Reller, J. M. Thomas, and D. A. Jefferson, Proc. R. Soc. London, Ser. A **394**, 223 (1984).

[21] J. J. Yeh and I. Lindau, At. Data Nucl. Data Tables **32**, 1 (1985).

[22] C. J. Ballhausen and H. B. Gray, *Molecular Orbital Theory* (Benjamin, New York, 1965).

[23] To do this we have weighted each contribution with the photoemission cross sections of Ref. 21 (reducing the O $2p$ cross section by a factor of 3 as in Ref. 14) and with the numbers of Mn $3d$ and O $2p$ electrons resulting from the calculations.